Giant dikes and dike-induced seismicity in a weak crust underneath Cerberus Fossae, Mars

Sam Rivas-Dorado[1*], Javier Ruíz[1], Ignacio Romeo[1]

[1]Departamento de Geodinámica, Estratigrafía y Paleontología, Universidad Complutense de Madrid, C/ Jose Antonio Novais, 12, 28040, Madrid, Spain.

*email: samuelrivas@ucm.es

Abstract

Cerberus Fossae is a long and narrow graben system located approximately 1000 km southeast of the Elysium bulge, Mars. These structures have long been thought to be dike-induced, and are the focus of renewed attention due to the detection of seismic activity in this area by InSight. Here we report that structural modeling and linear elastic fracture mechanics provide strong evidence that the Cerberus Fossae grabens are dike-related structures, and that their intrusion may have released significant amounts of seismic energy. The modeled dike apertures are between 176 and 745 m, and their aspect ratios are consistent with fluid-induced fractures formed in a weakened host rock. We observe densely fractured terrains in high-resolution images of the graben walls, confirming the presence of a weakened crust underneath Cerberus. We used dike geometry and adequate mechanical properties to calculate the source moment released by dike opening and inflation (M_d), which yielded values between $8 \cdot 10^{19}$ and $3.3\ 10^{22}$ Nm. From these we estimate that the Cerberus diking events may have expressed seismically with cumulative moment magnitudes (M_w) between 6.1 and 8.5. InSight has so far detected seismic events with M_w magnitudes as low as 1. Therefore, these results suggest that if emplacement of even smaller dikes than those inferred below Cerberus is currently taking place, intrusion-induced seismicity could be detected by InSight.

Keywords: dikes, graben, seismicity

Introduction

The InSight mission has detected multiple low-magnitude seismic events in the Elysium volcanic province, sourced both in and below the crust.. . Terrestrial dikes, which are narrow, long and tall magmatic intrusions, produce earthquakes of variable magnitude during their emplacement(e.g., Ayele et al., 2009; Calais et al., 2008; Maccaferri et al., 2016; Pallister et al., 2010; Passarelli et al., 2018; Sigmundsson et al., 2015; Wauthier et al., 2012), and therefore Martian dikes are expected to produce equivalent processes. Mars hosts ample evidence that supports the existence of large dike complexes (e.g., Goudy and Schultz, 2005; Wilson and Head III, 2002). The young Cerberus Fossae graben system is a good candidate to host these giant dikes at depth which, through one or several intrusion events, could have released significant amounts of seismic energy, similar to that observed in terrestrial diking events. Compelling evidence has been found supporting that long and narrow graben systems at Tharsis and Elysium regions were dike-induced (Rivas-Dorado et al., 2020; Schultz et al., 2004; Wilson and Head III, 2002), and therefore that dikes have played a significant role in the geodynamic evolution of Mars. Dikes have been proposed to be responsible not only of the formation of long and narrow grabens (Vetterlein and Roberts, 2010), but also of flooding events (Plescia, 2003; Russell and Head, 2003), the release of significant amounts of lava and gases to the surface (Jaeger et al., 2010; Yin Liu and Wilson, 1998) and, likely, of marsquakes produced during their emplacement. Indeed, marsquakes of M_w magnitudes between 7 and 8 have been proposed to have occurred in Cerberus Fossae and its surroundings, on the basis of fault rupture lengths estimated from boulder populations (Brown and Roberts, 2019; Roberts et al., 2012; Taylor et al., 2013).

InSight, which landed in Elysium Planitia in November 2018, has allowed the identification of deep marsquakes located underneath the Cerberus Fossae graben system (Figure 1) with M_w magnitudes of up to 3.8 (Banerdt et al., 2020; Brinkman et al., 2021; Giardini et al., 2020). On Earth, dikes are known to produce earthquake swarms with cumulative seismic moments between $8 \cdot 10^{12}$ and $4 \cdot 10^{19}$ Nm, equivalent to cumulative magnitudes between 2.3 and 6.7. Thus, if the graben system at Cerberus Fossae hosts giant dikes at depth, then it is expected that at least part of the energy released during their intrusion was expressed seismically. Furthermore, if dike intrusion were to occur at present day, then it is likely that this could be detected by the InSight seismometers.

In this work we report structural evidence supporting that the graben system at Cerberus Fossae was produced by giant dikes emplaced at depth. Also, we evaluate dike emplacement conditions and find that a weak host rock is needed to explain the dike aspect ratios, which is supported by the observation of highly fractured rocks in the graben walls. Finally, we estimate the possible seismic moment released by the emplacement of Cerberus dikes and conclude that the energy released during diking is comparable to some of the large recent terrestrial intrusion events, and that diking episodes could potentially be detected during the lifespan of the InSight mission. .

2. Methods

2.1. Cross section area balancing

Area balance is a well-established structural geology technique which uses the concept of cross-sectional area preservation between the undeformed and deformed states in geologic structures to determine the depth at which a structure is rooted, i.e., its detachment depth (Chamberlin, 1910), which is in this case an approximation for the top-dike depth. We selected PEDR tracks that crossed the selected Cerberus Fossae graben approximately at their center, and projected them to an orthogonal section to each structure to construct the final profiles. The method requires the present-day topography, the position of the upper fault tips, an assumed fault angle for normal faults (60°), the elevation of the graben floor, and two points which define the assumed initial topography (Figure 2a, and Supplementary Table 1). Then several parameters can be estimated: c, dike aperture, , D_{dg} and D_{dt}, the top-dike depth below the graben floor and topography, respectively and s_i, fault displacement (Figures 2b and c, Supplementary Figure 1, and

Supplementary Table 2). We also derive dike height, 2b, as two times the difference between the depth of the dike tip below the topography and the planetary Level of Neutral Buoyancy (LNB), assuming that the dike center is placed at said depth. Because the height of dikes in planetary crusts may be heavily dependent on density layering and and in order to capture this variability, we use two extreme but plausible depths for the LNB, 3 km and 20 km, to calculate minimum and maximum possible heights of dikes at Cerberus Fossae (see Supplementary Methods). For a full description of the area balance methodology and its associated uncertainties see Rivas-Dorado et al. (2020). The calculations were performed using a script of *python* code (*gryke*), which is made available (see Supplementary Methods).

2.2 Linear Elastic Fracture Mechanics (LEFM)

Firstly, we assume that the conditions required for LEFM apply, i.e., that dike intrusion occurred in a fully elastic, isotropic, homogeneous, isothermal medium. Multitude of previous studies have assumed host rock linear elasticity when addressing problems related to dike intrusion and have yielded successful results. In one of the earliest works in which LEFM was applied to geologic scenarios, Delaney and Pollard (1981) assumed host rock elasticity to model the thicknesses of minette dikes in Shiprock, New Mexico, and compared the results with field measurements of dike apertures. They found an excellent match between models and observations except for the terminal segments of the dikes, which they explained as caused by the interaction between adjacent dikes. The same fundamental theory has been used to obtain insights about dike apertures and dike emplacement conditions in more recent cases. For example, Kusumoto et al. (2013) modeled the apertures of basaltic-andesitic dikes in the Miyake-Jima volcano with very good fits between models and observations. Host rock elastic behavior has also been used in predictions of seismic release associated to dike opening. Bonaccorso et al.

(2017) positively correlated theoretical mechanical energies derived from elastic theory with measured cumulative seismic moments from 12 different recent diking episodes. They found that the released mechanical energy could be a valid proxy to estimate the real seismic release during dike intrusions. Modeling of faults and dikes using elastic dislocation theory has been used to calculate surface deformation in the events of the 2005-2010 Manda-Hararo sequence (e.g., Grandin et al., 2010; Wright et al., 2006), the 2009 Harrat-Lunayyir intrusion (e.g., Pallister et al., 2010; Xu et al., 2016), the 2014 Barđarbunga-Holuhraun espidode (e.g., Sigmundsson et al., 2015), or the 2011 Kamoamoa fissural eruption (Lundgren et al., 2013) . In all these cases, the modeled interferograms resulting from considering either dike only, fault only, or fault+dike deformation, reproduced very well the deformation measured by InSAR. In summary, the assumptions about the elastic behavior of the host rock behavior have produced results with predictive capabilities.

Based on the positive results from terrestrial studies previously discussed, and due to the uncertainties regarding the structure of the shallow crust in the Cerberus Fossae region, assuming a linear elastic behavior is a good *a priori* working assumption. Although much better estimates of the Martian crustal thickness are now available thanks to the InSight mission (Knapmeyer-Endrun et al., 2021), the actual layering of the upper crust remains unknown. Hesperian-Amazonian volcanic and clastic deposits cover most of southeastern Elysium, overlying denser Noachian terrains composed of older volcanic and sedimentary deposits (Pan et al., 2020; Tanaka et al., 2014). At latitudes between 0 and 30º, the shallow units potentially include a thick low-density permafrost layer (Clifford et al., 2010). Therefore, the shallow Martian crust in the Cerberus region may be rather heterogeneous at depth. When considering its thermal state, although there is evidence to suggest that volcanic activity occurred in the central Elysium region as recently as 2 Ma (Vaucher et al., 2009a), modern scientific research has not detected signs of present day volcanism. Therefore, because of the uncertainty on the nature of crustal layering at Cerberus Fossae and the absence of thermal anomalies at present day, we take a homogenous, isotropic, and isothermal medium as a valid initial assumption, conditions under which linear elasticity apply.

2.2.1 Stress intensity factor (K_I) and excess pressures (σ_e)

The stress intensity factor (K) is a parameter that measures the amount of energy required to open a given crack length (dike length, in this case), using the Griffith fracture criterion. Specifically, the stress intensity factor for opening-mode cracks (K_I) is expressed in its simplest form as (Lawn, 1993):

$$K_I = Y\sigma_e\sqrt{\pi a} \qquad (3)$$

where K_I is the stress intensity factor in Pa m$^{1/2}$, Y is a geometry factor dependent on crack shape, σ_e is excess pressure in Pa, defined as the difference between magma pressure (which opens the dike) and the stress acting orthogonal to the dike's walls (which resists dike opening and is opposite in direction to fluid pressure), and a is the fracture's half-length in m. K_I can also be calculated using the compact expression (Schultz, 2019):

$$K_I = \frac{E}{4(1-\upsilon^2)} c\sqrt{\frac{\pi}{a}} \qquad (4)$$

where E is Young's Modulus in Pa, v is Poisson's ratio (unitless), and c is maximum dike aperture in m. This equation is particularly useful when calculating K_I for a set of dike measurements, as it allows to use dike aperture, length and fundamental geomechanical properties.

We used the dike apertures inferred from area balance, dike lengths, assumed to be equal to the measured graben lengths, and the appropriate geomechanical properties in equation (4) to calculate K_I for the individual Cerberus dikes. Then, the K_I values obtained for each dike were used in equation (3) together with dike half-lengths to obtain σ_e for individual dikes. Both values are plotted in Figure 4. Wherever equation (3) was used, a geometry factor Y = 1 was assumed for simplicity, which is appropriate for single blade-like fractures in an infinite plate. Additionally, and for comparison, we also calculated K_I and σ_e for a dataset of modeled dikes in the nearby Elysium Fossae system (see Supplementary Methods for the treatment of the Elysium dataset). For Cerberus Fossae, the mechanical parameters used were a range of E and v values appropriate for a variably weakened host rock, E = 7.5 - 15 GPa and v = 0.10 - 0.25, and for Elysium Fossae those of an intact basalt, E = 63 GPa and v = 0.22. All K_I and σ_e values obtained for Cerberus are reported in Supplementary Table 3. Additionally, we used equation (3) to calculate the range of K_I and σ_e for fractures of fixed half-length between 5 and 75 km, which define the colored area in Figure 6.

2.2.2 Strain energy release rate (G_I) and minimum required dike energy (E_d)

The concept of strain energy release rate (or fracture propagation energy) for opening-mode cracks (G_I) was used to estimate the minimum energy required to open the dikes. G_I represents the energy required per new unit of fracture area at a fracture tip to drive its propagation or interaction with nearby fractures, and is given by (Lawn, 1993):

$$G_I = \frac{K_{I\,I}^2(1-v^2)}{E} \quad , \qquad (5)$$

where G_I is the strain energy release rate in J m^{-2}. This shows that G_I is dependent on K_I. To make more precise calculations which consider dike geometry we now use the extended K_I expression that accounts for the geometric corrections in embedded elliptical and semielliptical cracks (Anderson, 2005):

$$K_{Ic} = \sigma_e \sqrt{\frac{\pi a}{Q}} f(\phi), \qquad (6)$$

Where Q is a flaw shape parameter derived from elliptic integrals, and *f(ϕ)* is a function that accounts for the change of K_I along the crack front, and are given, respectively, by (Anderson, 2005):

$$Q = 1 + 1.464 \left(\frac{b}{a}\right)^{1.65}, \qquad (7)$$

$$f(\phi) = \left[sin^2\phi + \left(\frac{b}{a}\right)^2 cos^2\phi\right]^{1/4}, \qquad (8)$$

where *a* is the dike's half-length, *b* the dike's half-height ($D_h/2$), both in m, and ϕ is the angle of inspection relative to the fracture's axis (the axis along its length). Because we choose to inspect K_I at the long axis (where K_I is minimum), ϕ equals 0º and equation (8) reduces to a value of 1. G_I yields energy per unit area of new fracture length and consequently, knowing the crack area open by the dike allows to obtain a theoretical minimum total energy required to open the dike. The area ruptured by the dike is estimated by approximating the dike to an ellipse:

$$A_d = ab\pi, \qquad (9)$$

Where A_d is the approximated dike crack area. Substituting Equation (9) and Equation (6) in Equation (5) and rearranging we obtain:

$$E_d = (\pi a \sigma_e f(\phi))^2 b \frac{(1-\nu^2)}{QE}, \qquad (10)$$

where we refer to E_d as the required energy in Nm. Because E_d only takes into account the crack area created during dike opening, we use it as proxy for the minimum energy required to open the dikes. Equation (10) was used to calculate the dashed curves shown in Figure 7 using fixed parameters appropriate for the terrestrial and Martian cases. An average vertical extent of 6 km was used for the terrestrial dikes (blue dashed curve), whilst a value of 20 km was used to represent the Martian dikes (brown dashed curve). Constant values of σ_e = 25 MPa, E = 40 GPa, v = 0.25 and f(φ) = 0° were used for both curves. We also used eq. (10) to calculate E_d values for Cerberus Fossae using their lengths, estimated apertures, a range of heights, mechanical properties, and the the range of already calculated excess pressures. Because we defined minimum and maximum values for dike heights, E, and v, we calculate a range of E_d using combinations of these parameters. Using the minimum heights, E and v values we obtain the lower boundary for the energy ranges. Conversely, using the maximum dike height, E and v, we obtain the upper energy boundary. In all cases, we keep the rest of the parameters constant for each dike. All the obtained values are reported in Supplementary Table 3, and were used to plot the E_d ranges shown in Figure 7. We also used eq. (10) to calculate E_d values for all terrestrial dikes in which lengths, heights, and mechanical properties were available, using a constant σ_e = 25 MPa and f(φ) = 0° (the resulting values are reported in Supplementary Table 4).

2.3. Dike source moments (M_d)

The concept of source moment is used to provide an estimate of the maximum released energy by the intrusion of a dike. The dike moment M_d, i.e., the energy released via the inflation of a crack of arbitrary shape is given by (Mueller, 2001):

$$M_d = \left(\lambda + \frac{2}{3}\mu\right) V \qquad (11)$$

Where V is dike volume given by the product of 2a·2b·c, and λ and μ are the first and second Lamé's parameters, respectively, which can both be expressed in terms of E and v:

$$\lambda = \frac{Ev}{(1+v)(1-2v)} \quad (12)$$

$$\mu = \frac{E}{2(1+v)} \quad (13)$$

Therefore, equation (11) can be expressed in terms of E and v. Since volume is calculated from graben length equated to dike length, the modeled maximum aperture, and an estimated dike height, this is likely to represent a maximum possible dike volume.Because M_d allows to account for the energy associated with the volumetric expansion of the dike, we use it as a proxy to the maximum energy associated to dike opening. We used equation (11) to calculate the dotted curves shown in Figure 7 using fixed E, v, heights (2b) and apertures (c) appropriate to the terrestrial and Martian cases. For Mars (brown dotted curve), E = 40 GPa, v = 0.25, 2b =20 km, and c = 250 m (the average dike height and aperture for both the Cerberus and Elysium dikes). For Earth (blue dotted curve), E = 40 GPa, v = 0.25, 2b = 6 km, and c = 4 m (the average height and aperture of dikes as inferred from geodetic measurements reported in Supplementary Table 4). As with E_d, because we have previously defined minimum and maximum dike heights, E, and v, we use equation (11) to calculate a range of M_d values for the two extreme cases of heights and mechanical properties, keeping the rest of the dike parameters constant. The obtained ranges of M_d are shown in Figure 7 and are reported in Supplementary Table 3. . Equation (11) was also used to calculate an M_d for all terrestrial dikes for which volumes and mechanical properties were available (these values are plotted in Figure 7, and reported in Supplementary Table 4).

2.4. Seismic efficiency (ε) applied to estimating cumulative seismic moments (M_s)

The concept of seismic efficiency (ε) has been increasingly used in the past decade to understand how the energy budget is distributed during diking events. Seismic efficiency is defined as (Grandin et al., 2011):

$$\varepsilon = \frac{M_s}{M_g} \qquad (14)$$

where M_s is the cumulative seismic moment of all seismic events occurred during a diking event, and M_g is the total geodetic moment recorded during that event, usually calculated from ground deformation information (e.g., InSAR, Interferometric Synthetic Aperture Radar). Therefore, ε is a measure of how much of the total energy associated to dike intrusion was released seismically. The remainder of the energy is released aseismically, via either aseismic fault slip, fault creep, tensile opening (e.g., dike opening), or elastic deformation without rupture (Figure 3). Therefore:

$$M_g = M_s + M_a \qquad (15)$$

where M_a is the amount of energy released aseismically. In most of the documented terrestrial diking episodes (Supplementary Table 4) the portion of aseismic energy released by the dike represented, on average, 90% of the total aseismic energy, measured as an M_d/M_a ratio. Additionally, in many of these cases the reported dike energy represented not the majority, but the totality of the aseismic release. Therefore, to simplify the theoretical approach, we assume that all aseismic energy released during diking is associated to dike opening, i.e., that other mechanisms of aseismic energy release were absent, and thus that $M_a = M_d$ (Figure 3b). Then substituting equation (15) in equation (14) and rearranging yields:

$$M_s = \frac{\varepsilon M_d}{1-\varepsilon} \qquad (16)$$

This expression allows to estimate the cumulative seismic moment M_s of a diking event from the source moment M_d, an value of ε, and assuming that all aseismic energy was released via dike opening. Equation (16) was used on the M_d values calculated to estimate possible M_s at a range of seismic efficiencies derived from terrestrial examples. Seismic efficiencies for diking episodes on Earth were calculated where M_s and M_g were both available and are reported in Supplementary Table 4. , The average ε for dikes emplaced in rift zones is approximately 0.05 (e.g., Calais et al., 2008; Grandin et al., 2011; Nobile et al., 2012; Pallister et al., 2010), and we use this as a lower boundary of seismic efficiency. For dikes in volcanic arcs the average ε is around 0.3 (e.g., Bonforte et al., 2019; Cattania et al., 2017; Passarelli et al., 2018), and we use this as an upper boundary. Therefore, we use the range ε = 0.05 - 0.30 to calculate possible M_s values for the Cerberus dike intrusions. These M_s values at a range of seismic efficiencies obtained using the average M_d the Cerberus dikes define the colored polygon in Figure 7, and are reported in Supplementary Table 3b.

2.5. From moments to magnitudes

We use the expression in Hanks and Kanamori (1979), to move from the various energy measures calculated, E_d, M_d and M_s, both in Nm, to moment magnitude M_w, and vice versa:

$$M_{w,L,D,S} = \frac{2}{3} log M_i - 6.3 \quad , \qquad (17)$$

where M_i may be E_d, M_d or M_s in Nm.

3. Results and discussion

3.1 Structural modeling on dikes underneath Cerberus Fossae

Orthogonal cross sections across grabens in Cerberus Fossae (Figure 1) were constructed using the PEDR dataset of the MOLA instrument (Smith et al., 2001). Area balance, which assumes material conservation along each cross section, was performed on the inspected grabens in order to infer the geometry of the associated dikes (Methods, Section 2.1). Dike apertures, deduced from the addition of the heave for each of the bounding normal faults, are between 176 and 745 m. The top-dike tip depths, equivalent to the depth of the base of the upper layer where extension is accommodated by normal faulting, range from 280 to 813 m below the observed graben floor. The modeled dike heights are approximately between 4 and 39 km, depending on the LNB scenario consideredand km. Dike lengths, assumed to be equal to graben lengths measured on the surface, are between 30 and 140 km. The aperture to length relation of the inferred Cerberus dikes fits well with what is referred to as sublinear scaling, i.e., a relationship in the form $A = cL^{0.5}$ (Olson, 2003), which is characteristic of fluid-induced fractures as seen in many terrestrial fracture, vein and dike datasets (Figure 4). Therefore, our results are in line with the aspect ratios of known dike datasets measured in the field and support the possibility that the Cerberus graben host dikes at depth. Additionally, the displacement-length scaling of the modeled fault slips (between 153 and 757 m) matches with other Martian fault datasets, which provides additional support to our area balance results (Supplementary Figure 3).

Surface deformation on top of intruding dikes, expressed as ground subsidence, normal faulting, and tensile fracturing, has been observed and measured on Earth, in the field and through satellite data. Subsidence and normal faulting has been reported in recent diking events such as the 2005-2010 Manda-Harraro sequence (e.g., Grandin et al., 2010; Wright et al., 2006), the 2009 Harrat-Lunayyir intrusion (e.g., Pallister et al., 2010; Trippanera et al., 2019), or the 2014 Bardarbunga-Holuhraun crises (e.g., Ruch et al., 2016; Sigmundsson et al., 2015). In these cases, the calculated maximum dike apertures were between 4 and 10 m, measured ground subsidence was between 1 and 6 m, and fault slips did not surpass 1 m. These values are much smaller those calculated at Cerberus Fossae. However, successive intrusion events could produce dikes of much greater thickness and accumulate and fault slip, as suggested by later investigations of some of these events. Trippanera et al. (2019) reported the reactivation of pre-existing faults at Harrat-Lunayyir due to the 2009 event after a detailed structural mapping. Nobile et al., (2020) also investigated the post-diking history of this intrusion and identified aseismic subsidence of up to 1 mm/year following the crises. Thus, one or multiple events at Cerberus may have contributed to the creation of dikes of great thickness, deep graben, and faults with large slips. Models of dike intrusion and surface deformation further support this idea.

Numerical and analogue models have also shown graben development on top of intruding dikes. Through discrete element numerical experiments, Hardy (2016) modeled the evolution of dike-induced graben in a high-strength granular medium. By simulating the effects of tall dikes with a maximum half-width of 300 m, he obtained graben at surface with half-widths of 3 to 5 km, for dikes emplaced at 1.3 to 3.3 km depth. Analogue experiments in Trippanera et al. (2014), also show the formation of normal fault networks above a dike. They modeled dike intrusion by inserting 0.5-mm thick metal plates in a crushed cohesive sand, to a depth of 4 cm below their model surface. They injected up to 20 metal plates and produced a graben 2.85 cm wide, with nearly 40 mm of subsidence. Because in their models 1 cm ≡ 100 m, the thickness intruded was equivalent to 100 m, at a depth of 400 m, and resulted in graben 2.85 km width and 40 m deep. These modeled dike depths and apertures, and graben widths and depths, are in the same order of magnitude as the estimates for Cerberus Fossae.

Both field and satellite measurements of recent diking episodes, numerical and analogue models, suggest that dikes can produce graben at surface with dimensions consistent with those calculated for the Cerberus Fossae structures. This further supports the results obtained through area balance. However, some of these observations and experiments could also suggest that the giant Cerberus dikes may have required multiple events to form, as it has been inferred for giant terrestrial dikes based on geochemical evidence (e.g., Paktunç, 1987; Wilson, 1996). The obtained aspect ratios however suggest that a possible explanation for these thicknesses may be in the nature of the host rock.

The Cerberus Fossae dike system is structurally very similar to that of the nearby Elysium Fossae (Rivas-Dorado et al., 2020), with the key difference that the Cerberus grabens are significantly deeper (between 100 and 700 m) when comparing equivalent lengths. They are also much deeper than measured terrestrial dike-induced graben, and that most of those in the models previously discussed. This implies, when modeling through area balance, that the Cerberus dikes are significantly thicker (Supplementary Figure 4) than the Elysium structures with a similar length. Moreover, the obtained thickness estimates for Cerberus dikes imply much larger aspect ratios than all terrestrial dikes measured in outcrops and previously calculated Martian dikes, at around $A / L^{0.5} = 1.3$. (Figure 4). Terrestrial mafic dikes intruded in competent, intact rocks such as basalts and granitoids show aspect ratios of $A / L^{0.5} = 0.06$ (Babiker and Gudmundsson, 2004; Becerril et al., 2013; Coetzee and Kisters, 2017; Elshaafi and Gudmundsson, 2016; Schultz et al., 2008), whilst those intruded in fractured granites, uncompacted shales, and dacites in a fault damage zone (Chen et al., 2014; Delaney and Pollard, 1981; Ruz et al., 2020) show slightly larger aspect ratios around $A / L^{0.5} = 0.66$. Therefore, the aspect ratio of the

Cerberus dikes provides evidence of intrusion into weak host rocks. This is consistent with the changes observed in dike thicknesses intruded in heterogeneous sequences of weak and strong layers (e.g., Geshi et al., 2012). Moreover, magmas of similar and relatively high viscosity (ca. $2.5 \cdot 10^5$ Pa s) to large lava flows identified east of Cerberus Fossae (Vaucher et al., 2009b) are theorized to produce wider dikes, specially at high overpressures (Wada, 1994). Consequently, anomalously thick dikes may have been formed underneath Cerberus without requiring multiple intrusion events, favored by the presence of a weakened crust.

3.2 Evidence of a highly fractured crust beneath Cerberus Fossae

Geological mapping shows that the oldest units affected by the Cerberus graben system are highly cratered Hesperian-Noachian terrains (HNt,Tanaka et al., 2014) showing a rough chaotic texture (Figure 1). These terrains are characterized by the mixture of two units: (1) patchy terrains (basement outcrops of HNt), heavily cratered, and affected by a set of WNW-ESE penetrative fractures that, in some places, appear forming graben and (2) a smooth unit filling topographic lows (Figure 5a). The WNW-ESE fracture and graben set (striking parallel to the younger Cerberus grabens) does not affect younger units (AHv, lAv) that cover Hesperian Noachian terrains (HNt), while the Cerberus graben system affects all of them, being the youngest geological feature in the area.

A detailed inspection of the Hesperian-Noachian terrains (HNt) at the Cerberus graben walls shows the same two units separated by an unconformity (Figure 5b). On the top of the unconformity lies the smooth unit with horizontal layering exposed at the graben walls. Below, the deepest and oldest unit exposed in the area lays, being a rough basement characterized by a highly penetrative fracture fabric evident at m-scale outcrops.

The cross-cutting relationships, shown by regional geological mapping and detailed image inspection, indicate that the oldest and deepest unit in the area was affected by high-density penetrative fractures long time before the emplacement of Cerberus dikes (prior to the emplacement of AHv, lAv units). Therefore, a significant portion of the shallow crust in which the Cerberus dikes intruded is not an intact rock, but a damaged *rock mass* (Hoek and Brown, 1980).

3.3 Emplacement conditions in a weak host rock

We calculate the emplacement conditions of dikes in Cerberus Fossae by assuming an upper crust behaving as a rock mass rather than as intact rock through fundamental Linear Elastic Fracture Mechanics (LEFM). Individual stress intensity factors (K_I) and excess pressures (σ_e) calculated for the Cerberus Fossae dikes (see Methods, Section 2.2.1) are compared with theoretical predictions, which illustrate K_I and σ_e as a function of crack half-lengths between 5 and 75 km, similar to the lengths of the structures mapped (Figure 6). For comparison, we also show these parameters calculated using the same methodology for the Elysium dikes, for which the most appropriate geomechanical parameters of the host rock are those of an intact basalt (Rivas-Dorado et al., 2020).

We obtain K_I between 3.6 and 26.5 GPa $m^{1/2}$ and σ_e between 12 and 122 MPa for the Cerberus dikes, both in range of those obtained at Elysium. K_I is fundamentally dependent on crack geometry and excess pressure. Therefore, dikes with similar shapes formed by similar overpressures should yield similar stress intensity factors. Because both Cerberus and Elysium Fossae belong to the Elysium Rise plumbing system, they are expected to have formed under a similar range of magmatic pressures. Likewise, their maximum lengths do not surpass 150 km. Thus, similar stress intensity factors and excess pressures are expected for both set of structures. This can only be achieved when considering weak host rock properties at Cerberus (Figure 6).

There are several possible explanations for the presence of a weak host prior to dike emplacement. The HNt terrains of the Tartarus Montes, north of Cerberus Fossae, are severely cratered (Figure 3a). Impact deformation creates large damage zones both at surface and at depth, and modeling work suggests that craters with radii between 10 and 20 km may have damage zones extending up to ca. 7 km depth below the crater center (Collins et al., 2004; Kenkmann et al., 2014; Turtle et al., 2005).Interestingly, this depth range is consistent with the shallowest low-velocity layer identified at the location of InSight, which extends down to 7 to 10 km depth (Knapmeyer-Endrun et al., 2021). Thus, the upper crust is likely composed of large patchy areas of impact-induced fracture networks, in which the dikes may be partially or completely embedded, depending on their height.. Additionally, the highly rectilinear fracture patterns found at different scales (see previous section) suggest a possible tectonic origin for the observed intense rock fracturing.

Moreover, giant aqueous flows in the Athabasca Vallis region have been traced back to the southern Cerberus Fossae graben (graben 8 in Figure 1 is the main source of these outflows in Cassanelli and Head, 2018). As suggested by previous research, these could have been caused by dikes interacting with, and causing the catastrophic melt of, a shallow cryosphere (Head III et al., 2003; Cassanelli and Head, 2018). Some of these studies suggest that ice layers with thicknesses of several hundred meters may be sufficient to feed the Athabasca Vallis flows. However, underground ice deposits may be between 0 and 9 km in thickness at latitudes between 0 and 10º (Clifford et al., 2010), and thus potentially cover a significant portion of the vertical section intruded by the dikes. The strength of both pure ice and permafrost resembles more closely that of a rock mass rather than intact rock, with E values between 2 and 11 GPa (Arenson et al., 2015).

Consequently, these materials would behave similarly to impact-weakened basement, and would also allow for the accommodation of anomalously thick dikes.

Therefore, both a fractured crust caused by impacts and tectonic processes orthick layers of ice or permafrost, could have acted as a weak host for the Cerberus dikes, thus explaining the greater apertures achieved.

3.4 Uncertainties in dike heights in relation with crustal layering

If the dikes underneath Cerberus Fossae are partially embedded in a weakened shallow crust, then the presence of this density stratification may put constraints on dike heights, which are in turn a key parameters when calculating dike energies. Pollard and Townsend (2018) investigated the stability conditions of dikes intruded in both homogeneous and layered media and concluded that shorter dikes tended to be stable over a wider range of excess pressures and stress intensities than taller dikes. We used their equations 41 and 42, and considered density contrasts between 100 and 700 kg m^{-3} for dikes with half-heights between 1 and 19 km, to explore the stability of giant dikes under Martian conditions. In the case of a less dense layer resulting from the weakening of an original basement on top of intact bedrock, and therefore, of a relatively high density contrast, tall dikes with $c > 11$ km would only be stable (with $K_I > 0$ at both dike tips) at $\sigma_e > 9$ MPa, and even taller dikes with $c > 19$ km, at $\sigma_e > 15$ MPa. Our lower boundary for dike heights at Cerberus Fossae is approximately 4 km, when using the shallower LNB. Oppositely, our upper height limit is nearly 39 km when using the deep LNB, which is nearly at the 40 km maximum imposed by the thickness of the brittle crust (Jiménez-Díaz et al., 2020; Knapmeyer-Endrun et al., 2021). On the other hand, the excess pressures calculated here yield values between 12 and 122 MPa. Therefore, even in the case of a stratified crust, the tallest dike heights are possible and could be sustained by the relatively high excess pressures calculated. Thus, the calculated ranges of dike vertical extents are plausible, and provide insight into the amounts of energy released by the intrusions.

3.5 Energy boundaries and seismic moments of dike-induced marsquakes

We derive the minimum required energy for dike opening (E_d) from the strain energy release rate for mode-I cracks (see Methods, Section 2.2.2), and the maximum energy released by an opening dike (dike moment, M_d) from the source moment of an arbitrarily shaped crack (see Methods, Section 2.3). E_d for the Cerberus dikes is between $3.5\cdot10^{16}$ and $3.4\cdot10^{19}$ Nm and is consistently smaller than M_d for terrestrial dikes of equal length, and smaller than some of the terrestrial seismic releases (Figure 7). This is expected, as E_d represents the minimum energy needed for opening and does not account for dike inflation. Oppositely, M_d for the Cerberus dikes is generally larger than for terrestrial dike intrusions, ranging from $1.5\cdot10^{20}$ to $3.3\cdot10^{22}$ Nm, and larger than all terrestrial seismic releases(dike parameters and calculated energies for Cerberus Fossae are reported in Supplementary Table 3, whereas dike parameters and energies for the terrestrial dikes are compiled in Supplementary Table 4). We estimate the potential cumulative seismic moment (M_s) released by the dikes in the Cerberus system from M_d (see Methods, Section 2.4). Assuming that all aseismic energy during dike intrusion was released through dike opening in a single event and a range of values of seismic efficiency ε (0.05 to 0.3), we obtained for the Cerberus dikes average M_s between $5.39\cdot10^{19}$ and $1.22\cdot10^{21}$ Nm, equivalent to M_w magnitudes of 6.85 and 8.29 (Figure 7, colored polygon, Supplementary Table 3b). This range is above that of the seismic release of terrestrial dikes (Figure 7).

The lines which express M_d and E_d as a function of length for representative terrestrial and Martian dimensions (Section 2.2.2 and 2.3) define realistic upper and lower boundaries for the energy release of dikes. The terrestrial M_s values show a significant spread over lengths (0.8 to 60 km) and magnitudes (2.3 and 6.7), but lie between the M_d and . E_d lines (dotted and dashed blue lines, respectively, in Figure 7). Therefore, both energy quantities represent likely bounds for the maximum and minimum energy released during dike opening. Thus, it is expected that the seismic energy release of dike-related marsquakes calculated from the total dike moment would fall between the boundaries defined by E_d-M_d, when considering appropriate values of Martian dikes and intrusion conditions.

Additionally, a comparison between E_d and M_d for terrestrial events and their corresponding measured M_s yields strong correlations, which provides an additional tool to estimate the size of the Cerberus marsquakes between 7.7 and 9.4. These values overlaps with the range of the estimations previously presented based on the concept of seismic efficiency, and thus provides additional confidence in our calculations (see Supplementary Discussion, and Supplementary Figures 5 and 6).

3.6 Paleo and present-day dike seismicity

The cumulative seismic moments of the Cerberus Fossae diking events are equivalent to M_w magnitudes between 6.85 and 8.29 (Figure 7). These are remarkably similar to the magnitudes of paleo marsquakes in Cerberus Fossae and Grjota Valles estimated from approximations of surface fault rupture lengths derived from boulder trail populations, which are between 7.3 and 7.8 (Brown and Roberts, 2019; Roberts et al., 2012). These authors assumed that fault rupture occurred in a single event to derive their moment magnitudes. Because our results report the cumulative seismic moment released during the entirety of the intrusion, this may have been released via multiple faulting events, not necessarily through a single episode. The cumulative moment resulting from multiple smaller ruptures may be easily equivalent to a single, larger, faulting episode, which would allow to reconcile the two approximations. If the obtained displacements from area balance are entirely a result of accommodating dike extension at depth (through one or multiple events), then they can be used in expressions relating maximum displacement with moment magnitude in normal faults (Wells and Coppersmith1994, Table 2B). Total displacements between 100 and 800 m yield, using the corresponding equations, M_w between 8.02 and 8.67. These results ignore any contribution from strike-slip or buried normal faults but are also similar to the obtained M_w magnitudes at Cerberus. Moreover, the use of larger ε (e.g. 0.75) when calculating the Cerberus magnitudes would yield larger magnitudes even more similar to the previously discussed estimates. These results further suggest that large ancient marsquakes in these regions could have been produced by dike-related normal faulting.

The crustal and subcrustal marsquakes recently detected by InSight, with M_w between 1.3 and 3.8 (Giardini et al., 2020), correspond to single events consistent with background intraplate-like tectonic activity (Banerdt et al., 2020). Additionally, for the two well-recorded events in the Cerberus region, the preferred focal mechanisms are of normal faults striking between WNW-ESE and ENE-WSW (Brinkman et al., 2021). Therefore, these are both much lower magnitudes than those calculated in this study (Figure 7), and for the well-detected events, slightly oblique orientations to the Cerberus graben trend. However, it is conceivable that small intrusions could generate series of marsquakes in which many events would not be properly detected by the SEIS tool. If we consider all possible uncertainties regarding energy distribution during dike intrusion (see Supplementary Discussion), the source moment of a modest 25 km-long, 1 m-thick and 4km-tall dike (the shortest dike heights estimated), which accounted for 75% of the total aseismic moment release, at ε = 0.01, and using the lowest mechanical properties considered for the Cerberus area, could yield a cumulative seismic moment of $4.2 \cdot 10^{17}$ Nm, equivalent to an M_w of 4.12. This seismicity would be accommodated by multitude of smaller events occurring over a relatively short time (days to months, assuming a duration equivalent to terrestrial diking episodes), some of which may not be detected due to ambient noise or signal scattering. Therefore, these events would amount to cumulative seismic moments invariably smaller than the moments suggested by our work for a dike of a given size. This mode energy release may still be enough to allow detection, since InSight has detected quakes with magnitudes as low as 1. Seismicity would be produced by either strike-slip faults ahead of the dike tips (Ágústsdóttir et al., 2016), normal faults located above the upper dike tip (Xu et al., 2016), or normal faults at the lateral of the dikes (potentially reaching greater depths than the dike, e.g., Calais et al., 2008), which would yield focal mechanisms consistent with those already inferred from the InSight observations. Consequently, if an intrusion event with seismic expression were to occur during the lifespan of InSight, it stands to reason that researchers could identify it through these characteristics.

The results here presented show that the intrusion of giant dikes in a weak crust underneath Cerberus Fossae are a potential source of ancient and present-day seismicity. Furthermore, the identification of diking events through InSight observations would give a previously unthought way to understanding magmatic and tectonic processes currently ongoing on Mars.

Acknowledgements

The authors declare no financial conflict of interests. This research was funded by projects AMARTE II, PR75/18-21613 (research program Santander-UCM,), and TECTOMARTE, PGC2018-095340-B-I00 (Spanish Ministry of Science, Innovation and Universities).

References

Ágústsdóttir, T., Woods, J., Greenfield, T., Green, R.G., White, R.S., Winder, T., Brandsdóttir, B., Steinthórsson, S., Soosalu, H., 2016. Strike-slip faulting during the 2014 Bároarbunga-Holuhraun dike intrusion, central Iceland. Geophys. Res. Lett. 43, 1495–1503. https://doi.org/10.1002/2015GL067423

Anderson, T.L., 2005. Fracture Mechanics: Fundamentals and Applications, 3rd ed. Taylor & Francis, Boca Raton.

Arenson, L.U., Colgan, W., Marshall, H.P., 2015. Physical, Thermal, and Mechanical Properties of Snow, Ice, and Permafrost, in: Snow and Ice-Related Hazards, Risks, and Disasters. Elsevier, pp. 35–75. https://doi.org/10.1016/B978-0-12-394849-6.00002-0

Ayele, A., Keir, D., Ebinger, C., Wright, T.J., Stuart, G.W., Buck, W.R., Jacques, E., Ogubazghi, G., Sholan, J., 2009. September 2005 mega-dike emplacement in the Manda-Harraro nascent oceanic rift (Afar depression). Geophys. Res. Lett. 36, 1–5. https://doi.org/10.1029/2009GL039605

Babiker, M., Gudmundsson, A., 2004. Geometry, structure and emplacement of mafic dykes in the Red Sea Hills, Sudan. J. African Earth Sci. 38, 279–292. https://doi.org/10.1016/j.jafrearsci.2004.01.003

Baer, G., Hamiel, Y., 2010. Form and growth of an embryonic continental rift: InSAR observations and modelling of the 2009 western Arabia rifting episode. Geophys. J. Int. 182, 155–167. https://doi.org/10.1111/j.1365-246X.2010.04627.x

Banerdt, W.B., Smrekar, S., Banfield, D., Giardini, D., Golombek, M.P., Johnson, C., Lognonné, P., Spiga, A., Spohn, T., Perrin, C., Stähler, S., Antonangeli, D., Asmar, S., Beghein, C., Bowles, N., Bozdag, E., Chi, P., Christensen, U., John, C., Collins, G., Daubar, I., Dehant, V., Drilleau, M., Fillingim, M., Folkner, W., Garcia, R., Garvin, J., Grant, J., Grott, D.M., Grygorczuk, J., Hudson, T., Irving, J., Kargl, G., Kawamura, T., Kedar, S., King, S., Knapmeyer-Endrun, B., Knapmeyer, M., Lemmon, M., Lorenz, R., Maki, J., Margerin, L., McLennan, S., Michaut, C., Mimoun, D., Mittelholz, A., Mocquet, A., Morgan, P., Mueller, N., Murdoch, N., Nagihara, S., Newman, C., Nimmo, F., Panning, M., Pike, W., Plesa, A.-C., Rodriguez, S., Rodriguez-Manfredi, J.-A., Russell, C., Schmerr, N., Siegler, M., Stanley, S., Stutzmann, E., Teanby, N., Tromp, J., Driel, M. van, Warner, N., Weber, R., Wieczoreck, M., 2020. Initial Results from the InSight Mission on Mars. Nat. Geosci. 13, 183–189. https://doi.org/10.1038/s41561-020-0544-y

Becerril, L., Galindo, I., Gudmundsson, A., Morales, J.M., 2013. Depth of origin of magma in eruptions. Sci. Rep. 3, 1–6. https://doi.org/10.1038/srep02762

Bonaccorso, A., Aoki, Y., Rivalta, E., 2017. Dike propagation energy balance from deformation modeling and seismic release. Geophys. Res. Lett. 44, 5486–5494. https://doi.org/10.1002/2017GL074008

Bonforte, A., Guglielmino, F., Puglisi, G., 2019. Large dyke intrusion and small eruption: The December 24, 2018 Mt. Etna eruption imaged by Sentinel-1 data. Terra Nov. 31, 405–412. https://doi.org/10.1111/ter.12403

Brinkman, N., Stähler, S.C., Giardini, D., Schmelzbach, C., Khan, A., Jacob, A., Fuji, N., Perrin, C., Lognonné, P., Beucler, E., Böse, M., Ceylan, S., Charalambous, C., Clinton, J.F., van Driel, M., Euchner, F., Horleston, A., Kawamura, T., Knapmeyer-Endrun, B., Mainsant, G., Panning, M.P., Pike, W.T., Scholz, J., Robertsson, J.O.A., Banerdt, W.B., 2021. First focal mechanisms of marsquakes. J.

Geophys. Res. Planets. https://doi.org/10.1029/2020je006546

Brown, J.R., Roberts, G.P., 2019. Possible Evidence for Variation in Magnitude for Marsquakes From Fallen Boulder Populations, Grjota Valles, Mars. J. Geophys. Res. Planets 124, 801–822. https://doi.org/10.1029/2018JE005622

Calais, E., D'Oreye, N., Albaric, J., Deschamps, A., Delvaux, D., Déverchère, J., Ebinger, C., Ferdinand, R.W., Kervyn, F., Macheyeki, A.S., Oyen, A., Perrot, J., Saria, E., Smets, B., Stamps, D.S., Wauthier, C., 2008. Strain accommodation by slow slip and dyking in a youthful continental rift, East Africa. Nature 456, 783–788. https://doi.org/10.1038/nature07478

Cassanelli, J.P., Head, J.W., 2018. Large-scale lava-ice interactions on Mars: Investigating its role during Late Amazonian Central Elysium Planitia volcanism and the formation of Athabasca Valles. Planet. Space Sci. 158, 96–109. https://doi.org/10.1016/j.pss.2018.04.024

Cattania, C., Rivalta, E., Hainzl, S., Passarelli, L., Aoki, Y., 2017. A nonplanar slow rupture episode during the 2000 Miyakejima dike intrusion. J. Geophys. Res. Solid Earth 122, 2054–2068. https://doi.org/10.1002/2016JB013722

Chamberlin, R.T., 1910. The Appalachian Folds of Central Pennsylvania. J. Geol. 18, 228–251. https://doi.org/https://doi.org/10.1086/621722

Chen, N. hua, Dong, J. jin, Chen, J. yu, Dong, C. wan, Shen, Z. yue, 2014. Geometry and emplacement of the Late Cretaceous mafic dyke swarms on the islands in Zhejiang Province, Southeast China: Insights from high-resolution satellite images. J. Asian Earth Sci. 79, 302–311. https://doi.org/10.1016/j.jseaes.2013.10.001

Clifford, S.M., Lasue, J., Heggy, E., Boisson, J., McGovern, P., Max, M.D., 2010. Depth of the Martian cryosphere: Revised estimates and implications for the existence and detection of subpermafrost groundwater. J. Geophys. Res. 115, 1–17. https://doi.org/10.1029/2009je003462

Coetzee, A., Kisters, A.F.M., 2017. Dyke-sill relationships in Karoo dolerites as indicators of propagation and emplacement processes of mafic magmas in the shallow crust. J. Struct. Geol. 97, 172–188. https://doi.org/10.1016/j.jsg.2017.03.002

Collins, G.S., Melosh, H.J., Ivanov, B.A., 2004. Modeling damage and deformation in impact simulations. Meteorit. Planet. Sci. 39, 217–231. https://doi.org/10.1111/j.1945-5100.2004.tb00337.x

Delaney, P.T., Pollard, D.D., 1981. Deformation of Host Rocks and Flow of Magma during Growth of Minette Dikes and Breccia-bearing Intrusions near Ship Rock, New Mexico. USGS Prof. Pap. 1202 69.

Elshaafi, A., Gudmundsson, A., 2016. Volcano-tectonics of the Al Haruj Volcanic Province, Central Libya. J. Volcanol. Geotherm. Res. 325, 189–202. https://doi.org/10.1016/j.jvolgeores.2016.06.025

Geshi, N., Kusumoto, S., Gudmundsson, A., 2012. Effects of mechanical layering of host rocks on dike growth and arrest. J. Volcanol. Geotherm. Res. 223–224, 74–82. https://doi.org/10.1016/j.jvolgeores.2012.02.004

Giardini, D., Lognonné, P., Banerdt, W., Pike, W., Christensen, U., Ceylan, S., Clinton, J., Driel, M. van, Stähler, S., Böse, M., Garcia, R., Khan, A., Panning, M., Perrin, C., Banfield, D., Beucler, E., Charalambous, C., Euchner, F., Horleston, A., Jacob, A., Kawamura, T., Kedar, S., Mainsant, G., Scholz, J.-R., Smrekar, S., Spiga, A., Agard, C., Antonangeli, D., Barkaoui, S., Barrett, E., Combes, P., Conejero, V., Daubar, I., Drilleau, M., Ferrier, C., Gabsi, T., Gudkova, T., Hurst, K., Karakostas, F., King, S., Knapmeyer, M., Knapmeyer-Endrun, B., Ljorca-Cejudo, R., Lucas, A., Luno, L., Margerin, L., McClean, J., Mimoun, D., Murdoch, N., Nimmo, F., Nonon, M., Pardo, C., Rivoldini, A., Manfredi, J.A.R., Samuel, H., Schimmel, M., Stott, A.E., Stutzman, E., Teanby, N., Warren, T., Weber, R., Wieczorek, M., Yana., C., 2020. The Seismicity of Mars. Nat. Geosci. 13, 205–212. https://doi.org/10.1038/s41561-020-0539-8

Goudy, C.L., Schultz, R.A., 2005. Dike intrusions beneath grabens south of Arsia Mons, Mars. Geophys. Res. Lett. 32, 1–3. https://doi.org/10.1029/2004GL021977

Grandin, R., Jacques, E., Nercessian, A., Ayele, A., Doubre, C., Socquet, A., Keir, D., Kassim, M., Lemarchand, A., King, G.C.P., 2011. Seismicity during lateral dike propagation: Insights from new data in the recent Manda Hararo-Dabbahu rifting episode (Afar, Ethiopia). Geochemistry, Geophys. Geosystems 12. https://doi.org/10.1029/2010GC003434

Grandin, R., Socquet, A., Jacques, E., Mazzoni, N., De Chabalier, J.B., King, G.C.P., 2010. Sequence of rifting in Afar, Manda-Hararo rift, Ethiopia, 2005-2009: Time-space evolution and interactions between dikes from interferometric synthetic aperture radar and static stress change modeling. J. Geophys. Res. Solid Earth 115, 2005–2009. https://doi.org/10.1029/2009JB000815

Hanks, T.C., Kanamori, H., 1979. A Moment Magnitude Scale. J. Geophys. Res. 84, 2348–2350. https://doi.org/http://dx.doi.org/10.1029/JB084iB05p02348; doi:10.1029/JB084iB05p02348

Hardy, S., 2016. Does shallow dike intrusion and widening remain a possible mechanism for graben formation on Mars? Geology 44, 107–110. https://doi.org/10.1130/G37285.1

Head III, J.W., Wilson, L., Mitchell, K.L., 2003. Generation of recent massive water floods at Cerberus Fossae, Mars by dike emplacement, cryospheric cracking, and confined aquifer groundwater release. Geophys. Res. Lett. 30, 2–5. https://doi.org/10.1029/2003GL017135

Hoek, E., Brown, E.T., 1980. Empirical strength criterion for rock masses. J. Geotech. Eng. Div. 106, 1013–1035. https://doi.org/10.1016/0148-9062(81)90766-x

Jaeger, W.L., Keszthelyi, L.P., Skinner, J.A., Milazzo, M.P., McEwen, A.S., Titus, T.N., Rosiek, M.R., Galuszka, D.M., Howington-Kraus, E., Kirk, R.L., 2010. Emplacement of the youngest flood lava on Mars: A short, turbulent story. Icarus 205, 230–243. https://doi.org/10.1016/j.icarus.2009.09.011

Jiménez-Díaz, A., Egea-Gonzalez, I., Parro, L.M., Tasaka, M., Ruiz, J., 2020. The thermal structure and mechanical behavior of the Martian lithosphere. Icarus 113635. https://doi.org/10.1016/j.icarus.2020.113635

Kenkmann, T., Poelchau, M.H., Wulf, G., 2014. Structural geology of impact craters. J. Struct. Geol. 62, 156–182. https://doi.org/10.1016/j.jsg.2014.01.015

Klimczak, C., Schultz, R.A., Parashar, R., Reeves, D.M., 2010. Cubic law with aperture-length correlation: implications for network scale fluid flow. Hydrogeol. J. 18, 851–862. https://doi.org/10.1007/s10040-009-0572-6

Knapmeyer-Endrun, B., Panning, M.P., Bissig, F., Joshi, R., Khan, A., Kim, D., Lekić, V., Tauzin, B., Tharimena, S., Plasman, M., Compaire, N., Garcia, R.F., Margerin, L., Schimmel, M., Stutzmann, É., Schmerr, N., Bozdağ, E., Plesa, A.-C., Wieczorek, M.A., Broquet, A., Antonangeli, D., McLennan, S.M., Samuel, H., Michaut, C., Pan, L., Smrekar, S.E., Johnson, C.L., Brinkman, N., Mittelholz, A., Rivoldini, A., Davis, P.M., Lognonné, P., Pinot, B., Scholz, J.-R., Stähler, S., Knapmeyer, M., van Driel, M., Giardini, D., Banerdt, W.B., 2021. Thickness and structure of the martian crust from InSight seismic data, Science. https://doi.org/10.1126/science.abf8966

Kusumoto, S., Geshi, N., Gudmundsson, A., 2013. Aspect ratios and magma overpressures of non-feeder dikes observed in the Miyake-jima volcano (Japan), and fracture toughness of its upper part. Geophys. Res. Lett. 40, 1065–1068. https://doi.org/10.1002/grl.50284

Lawn, B., 1993. Fracture of brittle solids. Cambridge University Press, Cambridge. https://doi.org/10.1017/CBO9780511623127

Lundgren, P., Poland, M., Miklius, A., Orr, T., Yun, S.H., Fielding, E., Liu, Z., Tanaka, A., Szeliga, W., Hensley, S., Owen, S., 2013. Evolution of dike opening during the March 2011 Kamoamoa fissure eruption, Kīlauea Volcano, Hawai'i. J. Geophys. Res. Solid Earth 118, 897–914. https://doi.org/10.1002/jgrb.50108

Maccaferri, F., Rivalta, E., Passarelli, L., Aoki, Y., 2016. On the mechanisms governing dike arrest: Insight from the 2000 Miyakejima dike injection. Earth Planet. Sci. Lett. 434, 64–74. https://doi.org/10.1016/j.epsl.2015.11.024

Mueller, G., 2001. Volume Change of Seismic Sources from Moment Tensors. Bull. Seismol. Soc. Am. 91, 880–884.

Nobile, A., Cao, Y., Youssof, M., Trippanera, D., Passarelli, L., 2020. Post-diking deformation in Harrat Lunayyir (Saudi Arabia) from InSAR.

Nobile, A., Pagli, C., Keir, D., Wright, T.J., Ayele, A., Ruch, J., Acocella, V., 2012. Dike-fault interaction during the 2004 Dallol intrusion at the northern edge of the Erta Ale Ridge (Afar, Ethiopia). Geophys. Res. Lett. 39, 2–7. https://doi.org/10.1029/2012GL053152

Olson, J.E., 2003. Sublinear scaling of fracture aperture versus length: An exception or the rule? J. Geophys. Res. Solid Earth 108. https://doi.org/10.1029/2001jb000419

Paktunç, A.D., 1987. Differentiation of the Cuthbert Lake ultramafic dikes and related mafic dikes. Contrib. to Mineral. Petrol. 97, 405–416. https://doi.org/10.1007/BF00372003

Pallister, J.S., McCausland, W.A., Jónsson, S., Lu, Z., Zahran, H.M., El Hadidy, S., Aburukbah, A., Stewart, I.C.F., Lundgren, P.R., White, R.A., Moufti, M.R.H., 2010. Broad accommodation of rift-related extension recorded by dyke intrusion in Saudi Arabia. Nat. Geosci. 3, 705–712. https://doi.org/10.1038/ngeo966

Pan, L., Quantin-Nataf, C., Tauzin, B., Michaut, C., Golombek, M., Lognonné, P., Grindrod, P., Langlais, B., Gudkova, T., Stepanova, I., Rodriguez, S., Lucas, A., 2020. Crust stratigraphy and heterogeneities of the first kilometers at the dichotomy boundary in western Elysium Planitia and implications for InSight lander. Icarus 338, 113511. https://doi.org/https://doi.org/10.1016/j.icarus.2019.113511

Passarelli, L., Heryandoko, N., Cesca, S., Rivalta, E., Rasmid, Rohadi, S., Dahm, T., Milkereit, C., 2018. Magmatic or not magmatic? The 2015–2016 seismic swarm at the long-dormant jailolo volcano, west halmahera, Indonesia. Front. Earth Sci. 6, 1–17. https://doi.org/10.3389/feart.2018.00079

Plescia, J.B., 2003. Cerberus Fossae, Elysium, Mars: A source for lava and water. Icarus 164, 79–95. https://doi.org/10.1016/S0019-1035(03)00139-8

Pollard, D.D., Townsend, M.R., 2018. Fluid-filled fractures in Earth’s lithosphere: Gravitational loading, interpenetration, and stable height of dikes and veins. J. Struct. Geol. 109, 38–54. https://doi.org/10.1016/j.jsg.2017.11.007

Rivas-Dorado, S., Ruiz, J., Romeo, I., 2020. Subsurface Geometry and Emplacement

Conditions of a Giant Dike System in Elysium Fossae, Mars. J. Geophys. Res. Planets n/a, 2020JE006512. https://doi.org/https://doi.org/10.1029/2020JE006512

Roberts, G.P., Matthews, B., Bristow, C., Guerrieri, L., Vetterlein, J., 2012. Possible evidence of paleomarsquakes from fallen boulder populations, Cerberus Fossae, Mars. J. Geophys. Res. E Planets 117, 1–17. https://doi.org/10.1029/2011JE003816

Ruch, J., Wang, T., Xu, W., Hensch, M., Jónsson, S., 2016. Oblique rift opening revealed by reoccurring magma injection in central Iceland. Nat. Commun. 7, 1–7. https://doi.org/10.1038/ncomms12352

Russell, P.S., Head, J.W., 2003. Elysium-Utopia flows as mega-lahars: A model of dike intrusion, cryosphere cracking, and water-sediment release. J. Geophys. Res. 108. https://doi.org/10.1029/2002je001995

Ruz, J., Browning, J., Cembrano, J., Iturrieta, P., Gerbault, M., Sielfeld, G., 2020. Field observations and numerical models of a Pleistocene-Holocene feeder dyke swarm associated with a fissure complex to the east of the Tatara-San Pedro-Pellado complex, Southern Volcanic Zone, Chile. J. Volcanol. Geotherm. Res. 404, 107033. https://doi.org/10.1016/j.jvolgeores.2020.107033

Schultz, R.A., 2019. Geologic Fracture Mechanics. Cambridge University Press, Cambridge. https://doi.org/https://doi.org/10.1017/9781316996737

Schultz, R.A., Mège, D., Diot, H., 2008. Emplacement conditions of igneous dikes in Ethiopian Traps. J. Volcanol. Geotherm. Res. 178, 683–692. https://doi.org/10.1016/j.jvolgeores.2008.08.012

Schultz, R.A., Okubo, C.H., Goudy, C.L., Wilkins, S.J., 2004. Igneous dikes on Mars revealed by Mars Orbiter Laser Altimeter topography. Geology 32, 889–892.

https://doi.org/10.1130/G20548.1

Sigmundsson, F., Hooper, A., Hreinsdóttir, S., Vogfjörd, K.S., Ófeigsson, B.G., Heimisson, E.R., Dumont, S., Parks, M., Spaans, K., Gudmundsson, G.B., Drouin, V., Árnadóttir, T., Jónsdóttir, K., Gudmundsson, M.T., Högnadóttir, T., Fridriksdóttir, H.M., Hensch, M., Einarsson, P., Magnússon, E., Samsonov, S., Brandsdóttir, B., White, R.S., Ágústsdóttir, T., Greenfield, T., Green, R.G., Hjartardóttir, Á.R., Pedersen, R., Bennett, R.A., Geirsson, H., la Femina, P.C., Björnsson, H., Pálsson, F., Sturkell, E., Bean, C.J., Möllhoff, M., Braiden, A.K., Eibl, E.P.S., 2015. Segmented lateral dyke growth in a rifting event at Bárðarbunga volcanic system, Iceland. Nature 517. https://doi.org/10.1038/nature14111

Smith, D.E., Zuber, M.T., Frey, H. V., Garvin, J.B., Head III, J.W., Muhleman, D.O., Pettengill, G.H., Phillips, R.J., Solomon, S.C., Zwally, H.J., Banerdt, W.B., Duxbury, T.C., Golombek, M.P., Lemoine, F.G., Neumann, G.A., Rowlands, D.D., Aharonson, O., Ford, P.G., Ivanov, A.B., Johnson, C.L., McGovern, P.J., Abshire, J.B., Afzal, R.S., Sun, X., 2001. Mars Orbiter Laser Altimeter: Experiment summary after the first year of global mapping of Mars. J. Geophys. Res. Planets 106, 23689–23722. https://doi.org/10.1029/2000JE001364

Tanaka, K.L., Robbins, S.J., Fortezzo, C.M., Skinner, J.A., Hare, T.M., 2014. The digital global geologic map of Mars: Chronostratigraphic ages, topographic and crater morphologic characteristics, and updated resurfacing history. Planet. Space Sci. 95, 11–24. https://doi.org/10.1016/j.pss.2013.03.006

Taylor, J., Teanby, N.A., Wookey, J., 2013. Estimates of seismic activity in the Cerberus Fossae region of Mars. J. Geophys. Res. Planets 118, 2570–2581. https://doi.org/10.1002/2013JE004469

Trippanera, D., Acocella, V., Ruch, J., 2014. Dike-induced contraction along oceanic and continental divergent plate boundaries. Geophys. Res. Lett. 41, 7098–7104. https://doi.org/10.1002/2014GL061570

Trippanera, D., Ruch, J., Passone, L., Jónsson, S., 2019. Structural mapping of dike-induced faulting in harrat lunayyir (saudi arabia) by using high resolution drone imagery. Front. Earth Sci. 7, 1–23. https://doi.org/10.3389/feart.2019.00168

Turtle, E.P., Pierazzo, E., Collins, G.S., Osinski, G.R., Melosh, H.J., Morgan, J. V., Reimold, W.U., 2005. Impact structures: What does crater diameter mean? Spec. Pap. Geol. Soc. Am. 384, 1–24. https://doi.org/10.1130/0-8137-2384-1.1

Vaucher, J., Baratoux, D., Mangold, N., Pinet, P., Kurita, K., Grégoire, M., 2009a. The volcanic history of central Elysium Planitia: Implications for martian magmatism. Icarus 204, 418–442. https://doi.org/10.1016/j.icarus.2009.06.032

Vaucher, J., Baratoux, D., Toplis, M.J., Pinet, P., Mangold, N., Kurita, K., 2009b. The morphologies of volcanic landforms at Central Elysium Planitia: Evidence for recent and fluid lavas on Mars. Icarus 200, 39–51. https://doi.org/10.1016/j.icarus.2008.11.005

Vetterlein, J., Roberts, G.P., 2010. Structural evolution of the Northern Cerberus Fossae graben system, Elysium Planitia, Mars. J. Struct. Geol. 32, 394–406. https://doi.org/10.1016/j.jsg.2009.11.004

Wada, Y., 1994. On the relationship between dike width and magma viscosity. J. Geophys. Res. 99, 743–755. https://doi.org/10.1029/94jb00929

Wauthier, C., Cayol, V., Kervyn, F., D'Oreye, N., 2012. Magma sources involved in the 2002 Nyiragongo eruption, as inferred from an InSAR analysis. J. Geophys. Res.

Solid Earth 117, 1–20. https://doi.org/10.1029/2011JB008257

Wells, D.L., Coppersmith, K.J., 1994. New empirical relationships among magnitude, rupture length, rupture width, rupture area, and surface displacement. Bull. - Seismol. Soc. Am. 84, 974–1002.

Wilson, A.H., 1996. The Great Dyke of Zimbabwe. Dev. Petrol. 15, 365–402. https://doi.org/10.1016/S0167-2894(96)80013-3

Wilson, L., Head III, J.W., 2002. Tharsis-radial graben systems as the surface manifestation of plume-related dike intrusion complexes: Models and implications. J. Geophys. Res. 107, 5057. https://doi.org/10.1029/2001JE001593

Wright, T.J., Ebinger, C., Biggs, J., Ayele, A., Yirgu, G., Keir, D., Stork, A., 2006. Magma-maintained rift segmentation at continental rupture in the 2005 Afar dyking episode. Nature 442, 291–294. https://doi.org/10.1038/nature04978

Xu, W., Jónsson, S., Corbi, F., Rivalta, E., 2016. Graben formation and dike arrest during the 2009 Harrat Lunayyir dike intrusion in Saudi Arabia: Insights from InSAR, stress calculations and analog experiments. J. Geophys. Res. Solid Earth 121, 2837–2851. https://doi.org/10.1002/2015JB012505

Yin Liu, S., Wilson, L., 1998. Collapse pits due to gas release from shallow dikes on Mars, in: Lunar and Planetary Science Conference XXIX. https://doi.org/10.5860/choice.43sup-0240

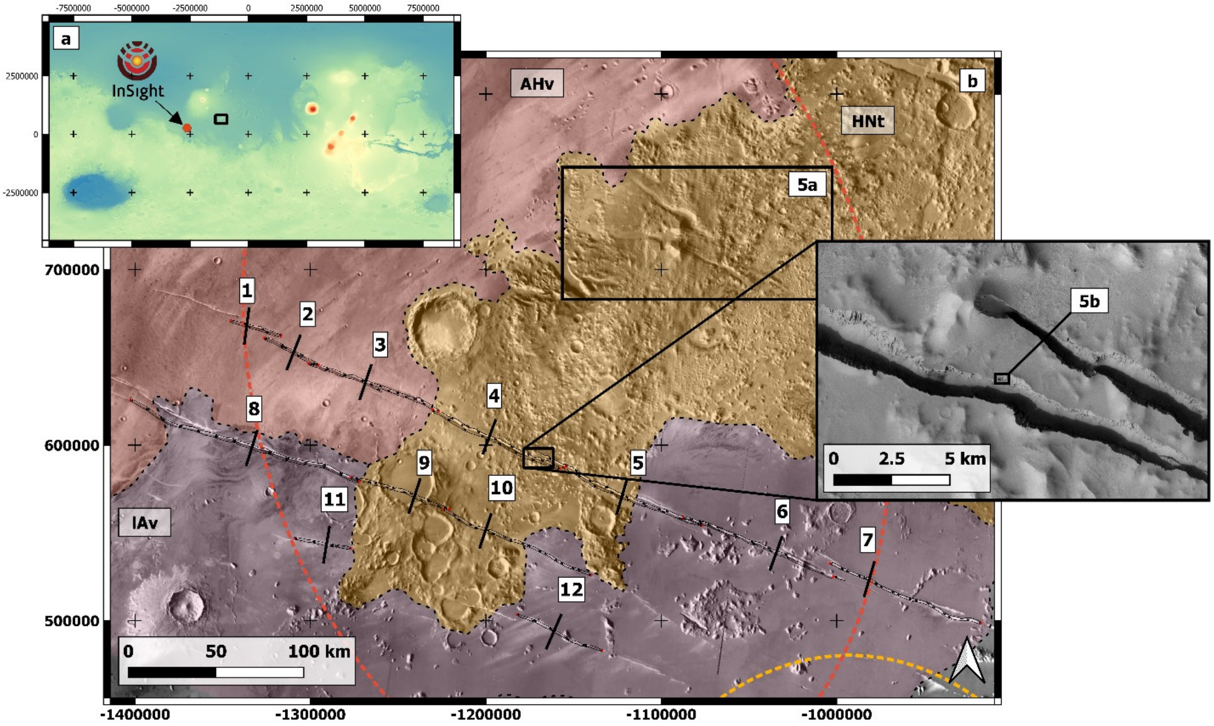

Figure 1. **Geological setting of the studied segments of the Cerberus Fossae graben system**. a) Global topographic map of Mars (MOLA, 435 m/px) where the study area and the location of InSight are indicated. Elevation unit is m. b) Mapped graben segments in northwestern Cerberus Fossae, with the location of the 12 cross sections studied, and the approximated uncertainty ellipses of seismic events S0235b (orange dashed ellipse, M_w = 3.1) and S0173a (yellow dashed line, M_w = 3.0, Giardini et al., 2020). Red dots indicate the extremes of the each graben segment mapped. The location of Figures 5a and b are indicated. A detail on CTX image d08_030378_1901_xn_10n199w (30 m/px) is shown, where Figure 5b is located. Units are from Tanaka et al. (2014). HNt = Hesperian-Noachian terrains, AHv = Amazonian-Hesperian volcanics, lAvf = Lower Amazonian volcanic flows, lAv = Lower Amazonian volcanics.

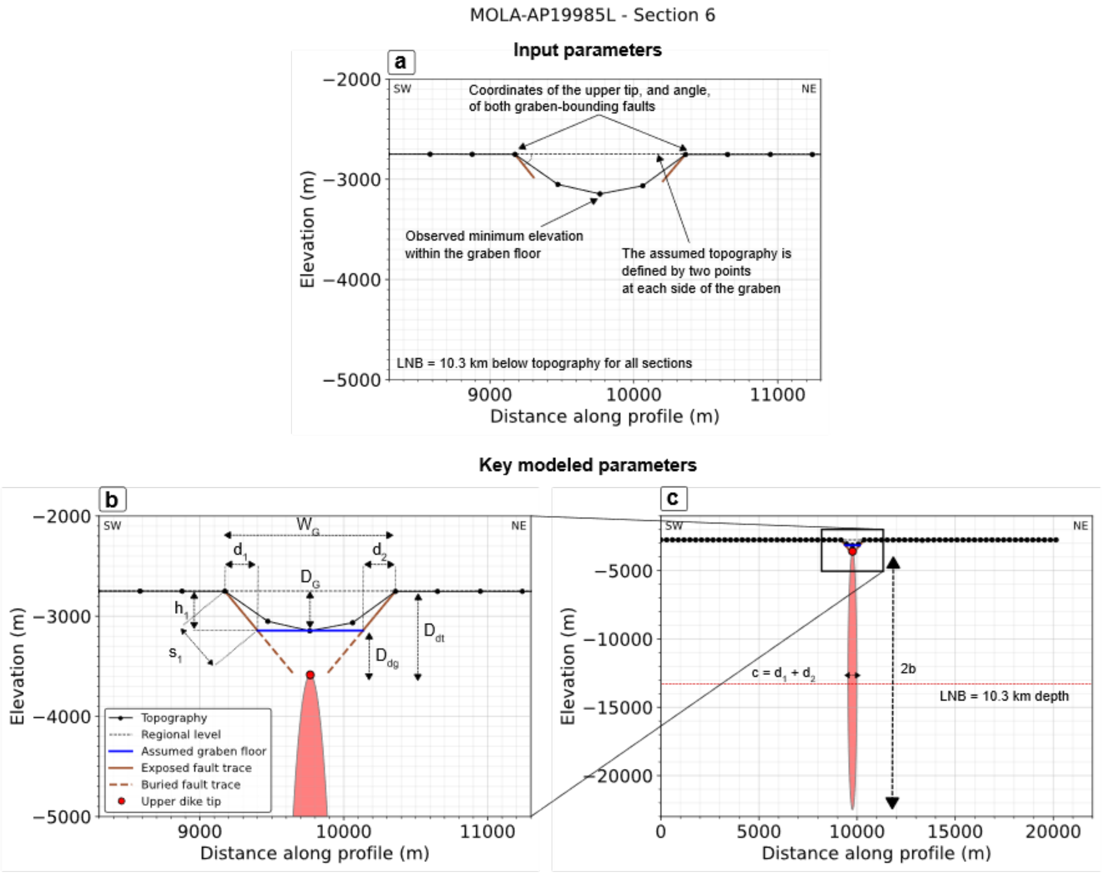

Vertical scale = Horizontal scale

Figure 2. Key input parameters required by area balance and output parameters returned in the model, illustrated by cross section 6. a) Input parameters indicated on the projected PEDR track AP19985L, used to create cross section 6. b) Detail on the most relevant parameters returned. W_G = Graben width, D_G = Graben depth, D_{dt} = Depth of dike below topography, D_{dg} = Depth of dike below graben floor, t_i = Fault throw, s_i = Fault slip, d_i = Fault heave. All elements of the visualization are indicated in the legend. c) Complete cross-sectional view of the modeled dike showing the rest of dike parameters. Maximum thickness is assumed at the center of the dike, at the level of neutral buoyancy (LNB). c = Dike aperture or thickness, 2b = Dike height or vertical extent.

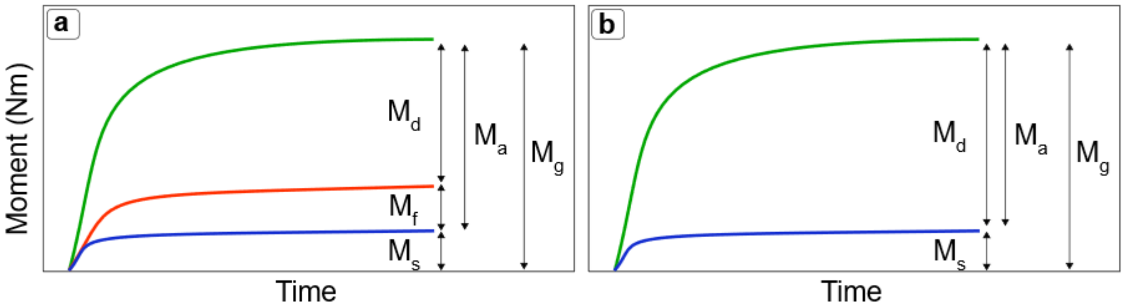

Figure 3. Distribution of the energy budget over time during dike intrusion. a) Energy allocation when both dike inflation and aseismic fault slip contribute to the aseismic moment. b) Energy distribution if no aseismic fault slip occurs and all aseismic moment is produced by the dike. M_s = Cumulative seismic moment, M_f = Aseismic fault moment, M_d = Dike moment, M_a = Aseismic moment, M_g = Geodetic moment. After Baer and Hamiel, (2010).

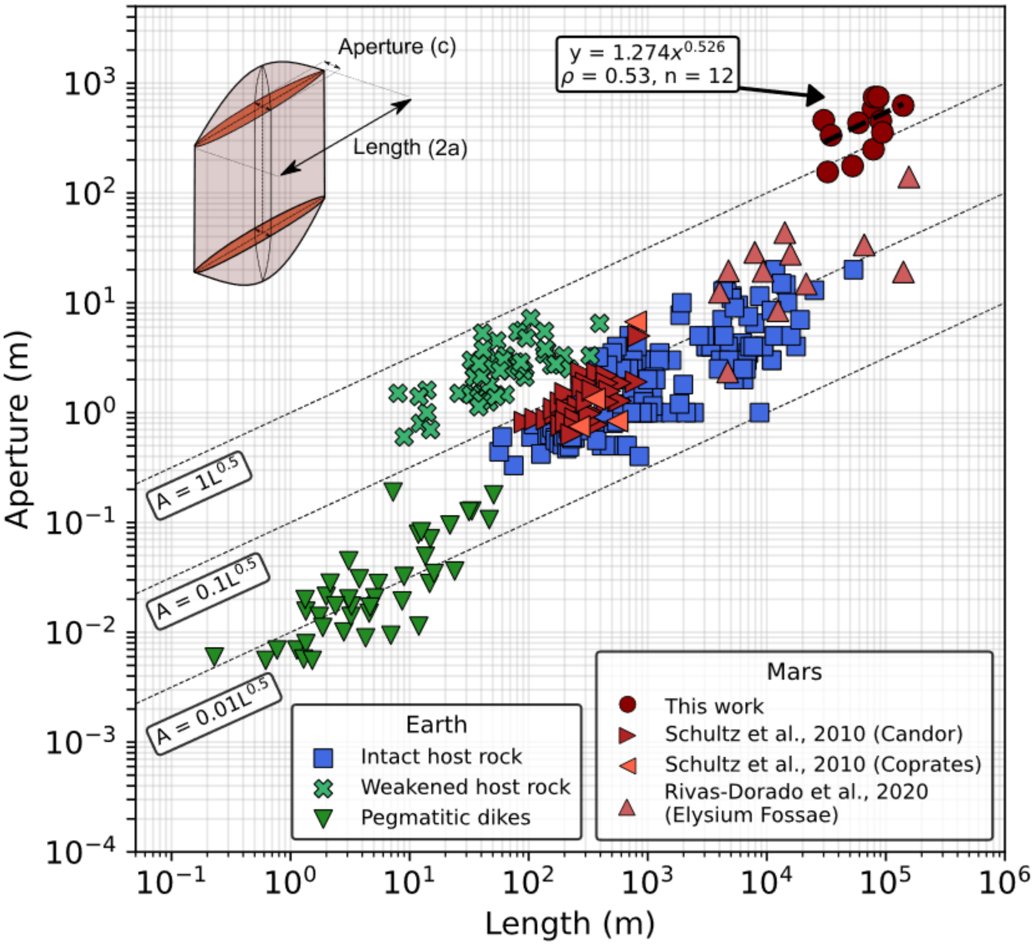

Figure 4. **Aperture-length scaling of multiple terrestrial and Martian dike datasets.** Terrestrial dikes are grouped in dikes intruded in intact host rocks (Babiker and Gudmundsson, 2004; Becerril et al., 2013; Coetzee and Kisters, 2017; Elshaafi and Gudmundsson, 2016; Schultz et al., 2008), weakened host rocks (Chen et al., 2014; Delaney and Pollard, 1981; Ruz et al., 2020), and pegmatitic dikes (Klimczak et al., 2010). Note that pegmatitic dikes and dikes intruded in a weak host plot at lower and larger aspect ratios, respectively, than those in intact hosts. Ideally, all dikes should fit to a scaling relationship of the type $A = c\ L^{-0.5}$. The regression of the Cerberus dataset to said function matches well with the expected scaling, as shown by the good linear correlation coefficient between aperture and length (ρ). Additionally, note the greater aspect ratios of

the Cerberus dikes, akin to the trend of dikes intruded in a weak host. The inset illustrates the dike geometry parameters plotted in this figure.

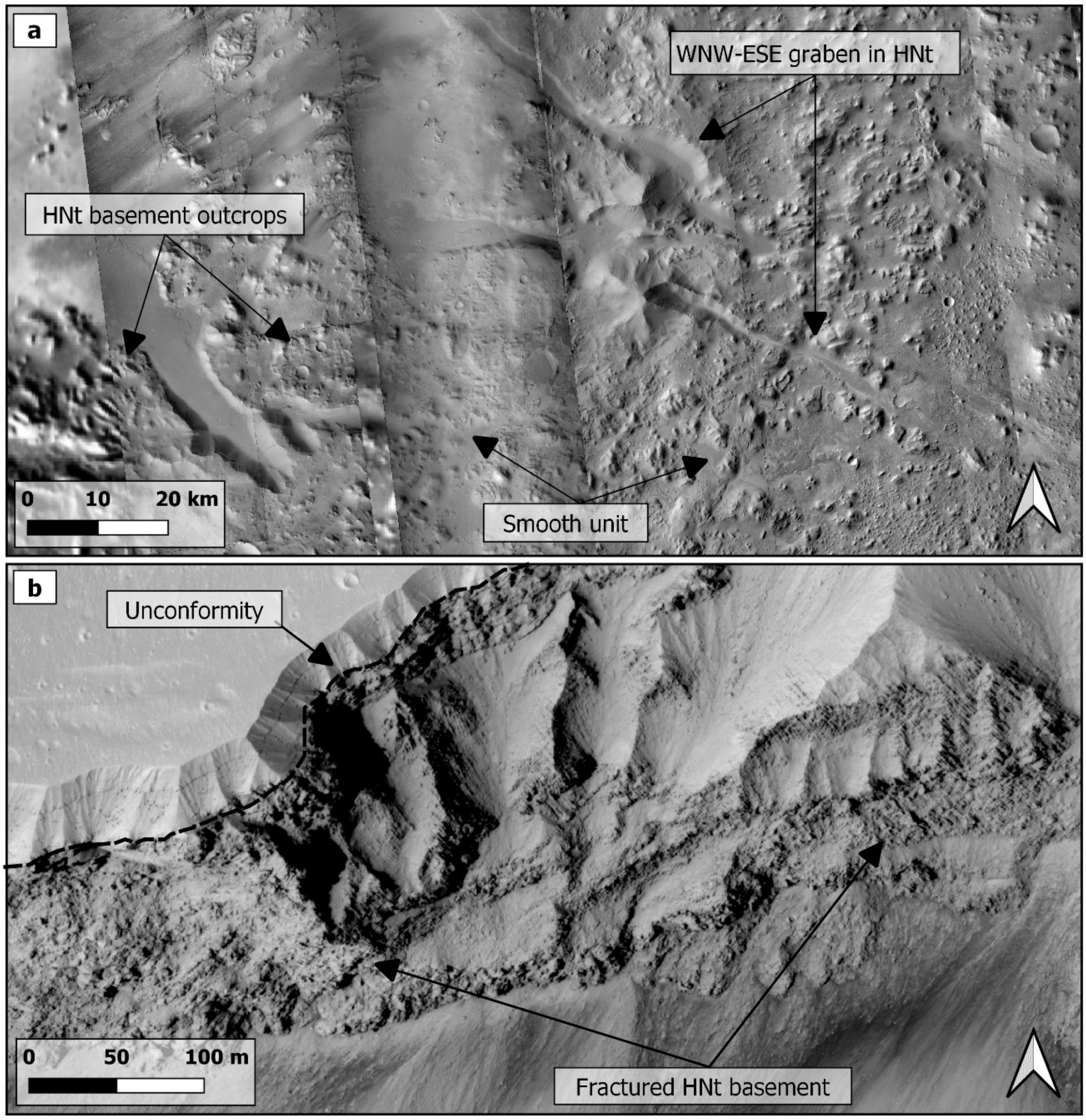

Figure 5. a) Detail on a composite of CTX images (30 m/px) showing heavily cratered, fractured and faulted terrains in unit HNt, with low-lying areas covered by a smooth unit. b) Detail on HiRISE image ESP_059349_1900_RED (25 cm/px) showing the northern wall of graben 4. A tens-of-meters thick, smooth layered unit is observed on top of a heavily fractured HNt basement, in which chaotic (left) and apparent sub-vertical penetrative fabrics (right) can be observed.

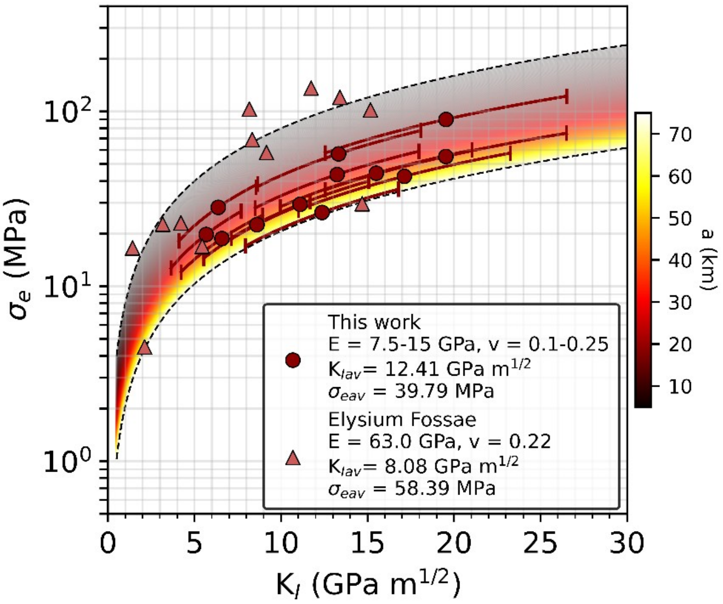

Figure 6. Excess pressures (σ_e) as a function of mode-I stress intensity factors (K_I) illustrating the emplacement conditions of large dikes in the Elysium Rise. For the Cerberus Fossae dikes, the points are at the average K_I and σ_e between the extreme E and v values considered, and the lines represent the full range of values. With the use of appropriate mechanical properties, the emplacement conditions of both dike sets overlap (K_I = 5 - 15 GPa $m^{1/2}$ and σ_e = 5 - 90 MPa), as may be expected for dikes of the same plumbing system. The colored region expresses the range of σ_e as a function of K_I for fractures of constant half-lengths (a) between 5 and 70 km (eq. 3). Average values of K_I and σ_e for each dataset are indicated in the legend.

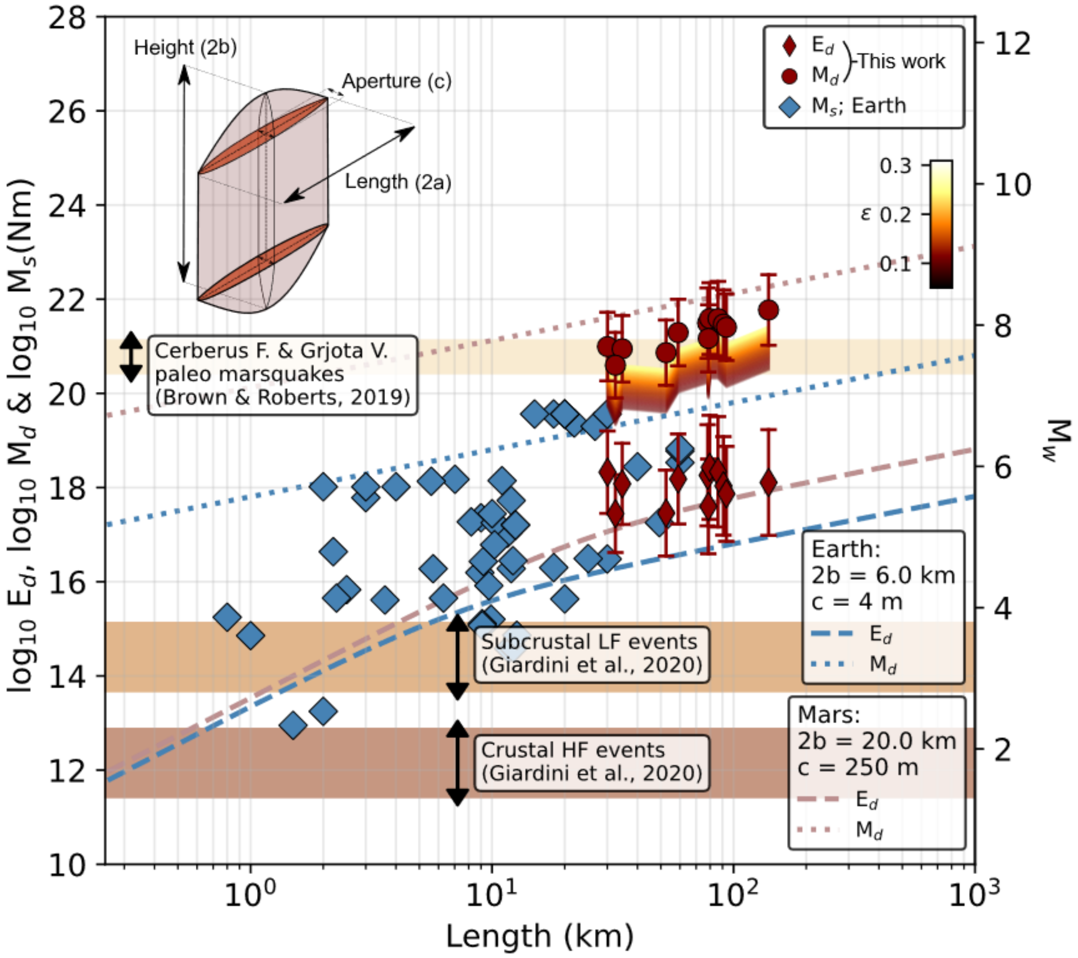

Figure 7. Dike moment (M_d),required energy (E_d) and cumulative seismic moment (M_s) as a function of dike length for the terrestrial and Cerberus Fossae dikes, together with the moment-magnitude ranges of past and present-day marsquakes. For the Cerberus dikes, the ranges of required energy (E_d) and moment (M_d) obtained using the minimum and maximum values of E, v, and heightare shown, with the average point plotted, are shown. Terrestrial diking events are shown collectively but correspond to various tectonic settings, and the datapoints correspond to cumulative seismic moments (M_s) (Supplementary Table 4, full set of references in Supplementary Information). The theoretical curves of E_d (eq. 10) and M_d (eq. 11) for both Earth and Mars use appropriate

average dike dimensions for each planet and illustrate the minimum and maximum energies associated to dike opening. For each curve and where applicable E = 40 GPa, v = 0.25, σ_e = 25 MPa, and f(φ) = 0º. Note that most cumulative seismic moments released in terrestrial diking events are between the minimum and maximum ranges defined by E_d and M_d. The colored polygon represents the range of M_s calculated from the average M_d for the Cerberus dikes for a range of ε between 0.05 0.3 as described in Section 2.4. For example, the longest Cerberus dike, at ε ≈ 0.2 would have released energy equivalent to $M_w \approx 8$. The range of magnitudes for the crustal and subcrustal events reported in Giardini et al. (2020), and the range of magnitudes of the Cerberus Fossae and Grjota Valles inferred from estimated surface rupture lengths in Brown & Roberts (2019), are indicated. The secondary y axis expresses energy as moment magnitude M_w. The inset illustrates the dike geometry parameters involved in the calculations of values in this figure.